Dynamic Modeling and Control of High-Speed Automated Vehicles for Lane Change Maneuver

Kai Liu, Jianwei Gong, *Member, IEEE*, Arda Kurt, *Member, IEEE*, Huiyan Chen, and Umit Ozguner, *Fellow, IEEE*

***Abstract*—Lane change maneuver of high-speed automated vehicles is complicated, since it involves highly nonlinear vehicle dynamics, which is critical for the driving safety and handling stability. Addressing this challenge, we present the dynamic modeling and control of high-speed automated vehicles for lane change maneuver. A nonlinear single-track vehicle dynamics model and a multisegment lane change process model are employed. Variable time steps are utilized for the vehicle model discretization to ensure a long enough prediction horizon, while maintaining model fidelity and computational feasibility. Accordingly, the control of lane change maneuver is addressed in two successive stages. First, by considering the lane change maneuver as primarily a longitudinal control problem, velocity profiles are determined to ensure the longitudinal safety of this maneuver. Then, the associated lateral control is generated with a model-predictive controller, taking the handling stability envelope, coupled tire forces, and environmental constraints into account. Simulations demonstrate the real-time ability and stable-handling capability of the proposed approach.**

***Index Terms*—High-speed automated vehicles, lane change maneuver, model predictive control, variable time-steps.**

I. Introduction

DUE to the advances in sensing and computing technology, automated vehicles have evolved significantly during the last decades. Many advanced driver assistance systems (ADAS), such as Adaptive Cruise Control (ACC) and Dynamic Stability Control (DSC), have been successfully integrated into commercial vehicles [1]. Furthermore, automated driving has demonstrated transformative potentials through ventures such as the DARPA grand and urban challenge [2], [3], and the Google self-driving car [4], etc. Nowadays, research efforts from both academia and industry have also targeted the high-speed automated vehicles, aiming to improve the driving safety and overall traffic efficiency [5]. Nevertheless, attaining high-speed automated driving still faces many problems. In particular, lane change maneuver in such conditions is a significant challenge.

Lane change maneuver of high-speed automated vehicles is challenging since it involves highly nonlinear vehicle dynamics. Therefore, a vehicle model with high fidelity is necessary to account for the dynamics related safety concerns, such as sidesilps caused by tire deformation and the maximal capabilities of tire-road friction. Besides, according to analysis of naturalistic lane change data, the duration time of a lane change maneuver mainly falls in 3–8 s [6]–[8]. This duration time necessitates a long enough prediction horizon to safely anticipate the movement of surrounding vehicles for hazard avoidance. Nevertheless, there is a dilemma between the model fidelity and time-step scales. On one hand, the vehicle model requires a short time-step to remain fidelity and fast response to the changes of environments. However, utilizing a short time-step for the whole prediction horizon would make the computational burden prohibitively heavy for real-time implementation. On the other hand, selecting a long time-step to realize sufficient prediction horizon with fewer time steps would degrade the model fidelity.

Other than vehicle dynamics modeling, control of high-speed automated vehicles for lane change maneuver is another challenge. Unlike the lane change of regular-speed automated vehicles, which is adequate to consider a collision-free trajectory, the vehicle handling stability and coupled tire forces become critical for driving safety of high-speed autonomated vehicles [9]–[11]. Thus, the dynamical safety constraints and the collision-free bounds should be systematically considered in the lane change maneuver [12]. However, these constraints may conflict with each other which propose further difficulties for the control of high-speed automated vehicles.

A. Related Works

A wide spectrum of dynamics modeling and control methods for lane change maneuver of automated vehicles have appeared in the literature [13]–[18]. Although these approaches do provide good results in their own respective applications, they either focus on relatively simple traffic environments or neglect the coupling effect between longitudinal and lateral motion. To account for surrounding vehicles and the coupled motions,

Manuscript received August 2, 2017; revised December 2, 2017 and March 26, 2018; accepted April 14, 2018. Date of publication June 1, 2018; date of current version August 23, 2018. This study was supported in part by the National Natural Science Foundation of China under Grants 51275041, 91420203 and 61703041 and in part by the China Scholarship Council (CSC) and the Fundamental Research Funds for the Central Universities. *(Corresponding author: Jianwei Gong.)*

K. Liu is with the Intelligent Vehicle Research Center, Beijing Institute of Technology, Beijing 100081, China, and also with the Center for Automotive Research, The Ohio State University, OH 43212 USA (e-mail: leoking1025@bit.edu.cn).

J. Gong and H. Chen are with the Intelligent Vehicle Research Center, Beijing Institute of Technology, Beijing 100081, China (e-mail: gongjianwei@bit.edu.cn; chen_h_y@bit.edu.cn).

A. Kurt and U. Ozguner are with the Center for Automotive Research, Department of Electrical Engineering, The Ohio State University, OH 43212 USA (e-mail: kurt.12@osu.edu; ozguner.1@osu.edu).

Color versions of one or more of the figures in this paper are available online at http://ieeexplore.ieee.org.

Digital Object Identifier 10.1109/TIV.2018.2843177

[19], [20] presented an effective lane change maneuvering method for automated vehicles with time-varying speeds. However, this method is derived from a kinematic vehicle model and didn't consider the dynamical safety constraints. Besides, variable time-steps is used for real-time motion planning [21].

Recent work has shown that Model Predictive Control (MPC) can be used to rigorously handling the multiple vehicle dynamics and safety constraints [22]. And the stability of this algorithm is also well studied [23]–[25]. To address the coupled tire force coupling effects, [26], [27] incorporate the Pacejka's magic formula tire model in the form of tire-road friction forces to capture the yaw dynamics and acceleration constraints. However, no active dynamical safety constraints are considered in these approaches. Alternatively, [28] proposed an approach to explicitly incorporated the stabilization criteria, such as stable handling envelope, into the MPC formulations. However, this approach still suffers from the underlying challenge that such constraints may be overly restrictive or conflict with each other, which may lead to collisions. By prioritizing collision avoidance, [29] proposed a method to systematically weight these sometimes conflicting objectives. If necessary, they even temporarily violate the stabilization criteria to avoid collisions. However, these applications are based on relatively simple environment settings, such as the obstacles are static in these scenarios and neglecting other vehicles. Moreover, taking the lane change maneuver as an instantaneous event and assuming constant speed during this maneuver does not consort with the real world scenarios.

B. Contributions

This paper presents the dynamic modeling and control of high-speed automated vehicles for lane change maneuver. A multi-segment lane change model is used to capture the lane change maneuver properties of adjusting the longitudinal position and velocity prior to initializing the lateral motion of this maneuver. The dynamical safety constraints are represented by the stable handling envelope and coupled tire forces envelope. Accordingly, an MPC controller is designed to realize collision avoidance while enforcing the dynamical safety constraints. Simulations validated the real-time ability and handling stability of the proposed approach. We claim two main contributions of this paper:

The first contribution is the variable time-steps for vehicle model discretization. The prediction horizon is divided into two portions. In the near portion, the vehicle model discretized with short time-step accurately captures the vehicle dynamics. In the latter portion, the vehicle model discretized with long time-step and first-order hold (FOH) method provides reduced modeling errors over the prediction horizon while mitigating the computational burden. In this way, the variable time-steps ensure a long enough prediction horizon while maintaining model fidelity and computational feasibility.

Another contribution is stabilization control of high-speed automated vehicles for lane change maneuver while accounting for and adapting to the surrounding vehicles. The lane change maneuver is addressed in two successive stages. First, by conservatively assuming a fixed lateral motion time, a proper longitudinal acceleration profile is determined. Then, the lateral control is designed as an MPC problem to systematically mediated the dynamical safety constraints and the environmental constraints.

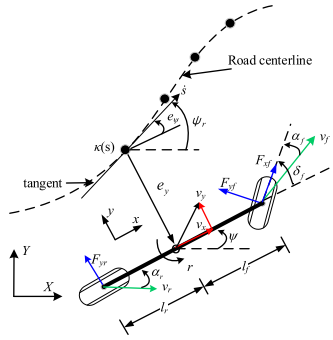

Fig. 1. A diagram of dynamical single-track vehicle model.

Throughout the paper, the following assumptions are made:

- The automated vehicle is equipped with low-level control systems capable of performing the optimized controls;
- Since the decision-making mechanism has been widely discussed in previous studies, it is not included in this work. The lane change maneuver request and the potential inter-vehicle traffic gap are given manually;
- We hypothesize adequate knowledge about the traffic environment, such as relative speed and position of surrounding vehicles. This is possible due to the advantages in communication forms such as V2V, V2I, etc.

The remainder of this paper is organized as follows: Section II introduces the modeling of vehicle dynamics and lane change process. Section III describes the decoupled longitudinal and lateral control of high-speed automated vehicles for lane change maneuver. Section IV shows the simulation results. Conclusions are drawn in Section V.

II. Dynamic Modeling of Lane Change Maneuver

A. Single-Track Vehicle Dynamics Modeling

Considering a front-wheel driven automated vehicle, a single-track vehicle model in combination with a semi-empirical tire model is employed, as illustrated in Fig. 1. Table I provides an overview of the employed model parameters.

The vehicle dynamics and relative motion with respect to the road curvilinear coordinate system can be described as

$$\dot{v}_x = a_x \tag{1a}$$

$$\dot{v}_y = r\dot{v}_x + \frac{1}{m}(F_{yf} + F_{yr}) \tag{1b}$$

$$\dot{r} = \frac{1}{I_z}(l_f F_{yf} - l_r F_{yr}) \tag{1c}$$

$$\dot{e}_\psi = r \tag{1d}$$

$$\dot{e}_y = v_x e_\psi + v_y \tag{1e}$$

$$\dot{s} = v_x \tag{1f}$$

with the small angle assumptions of $e_\psi \approx 0$ and $\delta_f \approx 0$.

TABLE I
EMPLOYED MODEL PARAMETERS

Symbol	Description
m	vehicle mass
I_z	Yaw moment of inertia (vertical axis)
μ	Maximum tire/road friction coefficient
l_f, l_r	Distance between CoG and front/rear axle, respectively
v_x, v_y	Longitudinal/lateral velocity at CoG in veh. ref. frame
ψ, ψ_r	Heading angle of vehicle and road centerline
r	Yaw rate
e_ψ	Difference angle between vehicle and road centerline
e_y	The lateral distance between CoG and road centerline
δ_f	Actual wheel steering angle at the front axle
a_x	Longitudinal acceleration of the vehicle
κ	Road centerline curvature, assumed to be zero.
C_{α_r}	Tire cornering stiffness
α_f, α_r	Sideslip angle at front/rear tire
F_{xf}	Applied longitudinal force at the front tire
F_{yf}, F_{yr}	Applied lateral forces at the front/rear tire, respectively
F_{zf}, F_{zr}	Vertical tire load at front/rear tire, respectively

For the tire force terms in (1), a modified brush tire model presented in form (2) by Pacejka is used to approximate the effect of tire force coupling.

$$F_y = \begin{cases} -C_\alpha \tan\alpha + \frac{C_\alpha^2}{3\eta\mu F_z} |\tan\alpha| \tan\alpha \cdots \\ -\frac{C_\alpha^3}{27\eta\mu^2 F_z^2} \tan^3\alpha, |\alpha| < \arctan\left(\frac{3\mu F_z}{C_\alpha}\right) \\ -\eta\mu F_z \mathrm{sgn}\alpha, \text{ otherwise} \end{cases}$$
$$= \boldsymbol{f}_{\text{coupled}}(\alpha, F_x) \tag{2}$$

with the derating factor $\eta (0 \le \eta \le 1)$ be computed as

$$\eta = \frac{\sqrt{(\mu F_z)^2 - (F_x)^2}}{\mu F_z} \tag{3}$$

Neglecting the lateral load transfer, the vertical loads account for the longitudinal load transfer effects are

$$F_{zf} = \frac{mgl_r - mha_x}{l_f + l_r}, F_{zr} = \frac{mgl_f + mha_x}{l_f + l_r} \tag{4}$$

The tire slip angle in the front (α_f) and rear (α_r) can be linearized using small angle approximations:

$$\alpha_f = \arctan\left(\frac{v_y + l_f r}{v_x}\right) - \delta_f \approx \frac{v_y + l_f r}{v_x} - \delta_f \tag{5a}$$

$$\alpha_r = \arctan\left(\frac{v_y - l_r r}{v_x}\right) \approx \frac{v_y - l_r r}{v_x} \tag{5b}$$

It's noted that the single-track model can be decoupled into the longitudinal dynamics (1a) and (1f), and the corresponding lateral dynamics, (1b)–(1e). The longitudinal dynamics (1a) and (1f) can thus be formulated as a two-state space model

$$\dot{\boldsymbol{\varpi}} = \begin{bmatrix} 0 & 1 \\ 0 & 0 \end{bmatrix} \boldsymbol{\varpi} + \begin{bmatrix} 0 \\ 1 \end{bmatrix} a_x \tag{6}$$

where $\boldsymbol{\varpi} = [s, v_x]^T$ is the longitudinal state vector and a_x is the longitudinal control input.

As to the lateral dynamics, the nonlinearity of tire forces, contained in the terms of F_{yf} and F_{yr}, poses a significant challenge to real-time optimization. Regarding to this problem, we use front tire force (F_{yf}) rather than front wheel steer angle (δ_f) to describes the vehicle's lateral behavior. Use of F_{yf} as the model input allows for a linear lateral vehicle model which considers front tire coupling effects. And the input F_{yf} can be mapped to front wheel steering angle δ_f using (2) and (5a):

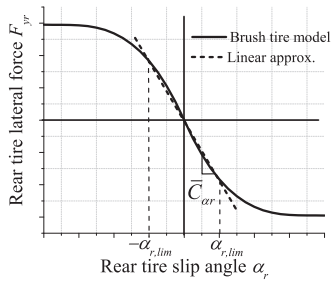

Fig. 2. Brush tire model with linear approximation.

$$\delta_f = \frac{v_y + l_f r}{v_x} - \boldsymbol{f}^{-1}_{\text{coupled}}(F_{yf}, F_{xf}) \tag{7}$$

The longitudinal front tire force F_{xf} can be computed as

$$F_{xf} = ma_x + F_R \tag{8}$$

where, F_R represents the dissipative forces such as aerodynamic drag and friction force. Because $\eta\mu$ appears in (2) as a derated surface friction, therefore, F_{xf} here serves only to augment the surface friction coefficient. Thus, $\boldsymbol{f}^{-1}_{\text{coupled}}(F_{yf}, F_{xf})$ can be implemented as a 2D lookup table.

The rear lateral tire forces (F_{yr}) can be approximated as

$$F_{yr} = \bar{C}_{\alpha r}\alpha_r \tag{9}$$

where $\bar{C}_{\alpha r}$ is the equivalent cornering stiffness at $\alpha_r = 0$. This relationship linearizes the brush tire force model in the linear region of the tire characteristics functions, as illustrated in Fig. 2. This linearization will lead to diverging from the actual tire forces quite significantly at high slip values, however, this problem may be mitigated by enforcing a tire slip angle constraint, $\alpha_{r,lim}$. This approximation is validated by the stability constraints as discussed in Section III.

The equations of (1b) and (1c) can now be rewritten as affine functions of the lateral control input, F_{yf}:

$$\dot{v}_y = \frac{1}{m}\left[F_{yf} + \bar{C}_{\alpha_r}\left(\frac{v_y - l_r r}{v_x}\right)\right] - r v_x \tag{10}$$

$$\dot{r} = \frac{1}{I_z}\left[l_f F_{yf} - l_r \bar{C}_{\alpha_r}\left(\frac{v_y - l_r r}{v_x}\right)\right] \tag{11}$$

Combining (5), (10) and (11), a linear time-varying vehicle model in state-space representation can be expressed as

$$\dot{\boldsymbol{\xi}} = \mathbf{A}\boldsymbol{\xi} + \mathbf{B}F_{yf} \tag{12}$$

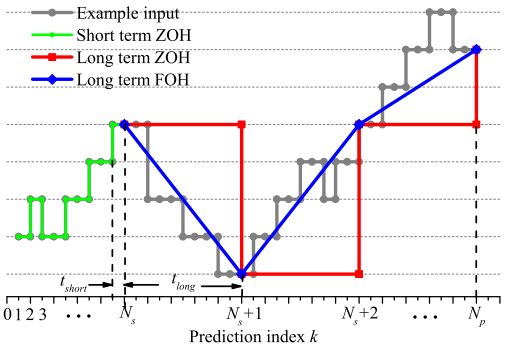

Fig. 3. Model discretization in two-time scale prediction horizon.

with

$$\mathbf{A} = \begin{bmatrix} \frac{\bar{C}_{\alpha_r}}{m v_x} & -\frac{\bar{C}_{\alpha_r} l_r}{m v_x} - v_x & 0 & 0 \\ -\frac{\bar{C}_{\alpha_r} l_r}{I_z v_x} & \frac{\bar{C}_{\alpha_r} l_r^2}{I_z v_x} & 0 & 0 \\ 0 & 1 & 0 & 0 \\ 1 & 0 & v_x & 0 \end{bmatrix} \mathbf{B} = \begin{bmatrix} \frac{1}{m} \\ \frac{l_f}{I_z} \\ 0 \\ 0 \end{bmatrix}.$$

where $\boldsymbol{\xi} = \begin{bmatrix} v_y & r & e_\psi & e_y \end{bmatrix}^T$ is the lateral state vector and F_{yf} is the lateral control input.

B. Variable Time-Steps for Model Discretization

This work uses two-time scales in the prediction horizon to discrete the longitudinal and lateral dynamics model. As illustrated in Fig. 3, the whole prediction horizon includes N_p discretized time steps, and it is split into two portions at the N_s^{th} time step. The initial portion is comprised of small time steps, t_{short}, which equals to the MPC based low-level controller's execution period, to accurately capture near-term vehicle behavior. The latter portion is comprised of larger time steps, t_{long}, to extend the horizon to incorporate upcoming traffics in the long-term.

For the discretization of lateral dynamics (12), zero-order hold (ZOH) and first-order hold (FOH) methods are applied to the initial portion and latter portion of the prediction horizon, respectively. For the initial portion $k = 0, \ldots, N_s$, the lateral vehicle model is discretized with t_{short} and ZOH method. By considering the augmented state vector $\mathbf{z}_s = \begin{bmatrix} \boldsymbol{\xi} & F_{yf} \end{bmatrix}^T$, the short-term model evolves according to the system:

$$\begin{bmatrix} \dot{\boldsymbol{\xi}}(k) \\ \dot{F}_{yf}(k) \end{bmatrix} = \begin{bmatrix} \mathbf{A}^k & \mathbf{B}^k \\ 0 & 0 \end{bmatrix} \begin{bmatrix} \boldsymbol{\xi}(k) \\ F_{yf}(k) \end{bmatrix} = \mathbf{G}_s^k \mathbf{z}_s(k) \tag{13}$$

where, $\mathbf{A}^k$ and $\mathbf{B}^k$ are computed with pre-defined velocity profiles. This system (15) can be discretized by taking the matrix exponential of $\mathbf{G}_s^k t_{\text{short}}^k$

$$\begin{bmatrix} \boldsymbol{\xi}(k+1) \\ F_{yf}(k+1) \end{bmatrix} = \begin{bmatrix} \mathbf{A}_s^k & \mathbf{B}_s^k \\ 0 & 1 \end{bmatrix} \begin{bmatrix} \boldsymbol{\xi}(k) \\ F_{yf}(k) \end{bmatrix} \tag{14}$$

with $\mathbf{A}_s^k = \mathbf{I} + \mathbf{A}^k t_{\text{short}}$ and $\mathbf{B}_s^k = \mathbf{B}^k t_{\text{short}}$. From the second row of (14), the ZOH assumption $F_{yf}(k+1) = F_{yf}(k)$ is verified. The first row of (14) gives the discrete model:

$$\boldsymbol{\xi}(k+1) = \mathbf{A}_s^k \boldsymbol{\xi}(k) + \mathbf{B}_s^k F_{yf}(k) \tag{15}$$

Fig. 3 illustrates the comparison of different model discretization methods and an example control input sequence is shown in gray. The control input assumed by the discrete model (15) is shown in green. We can see that it provides an accurate model to match the example control input in gray. This is because the lower-controller inherently attempts to hold F_{yf} constant over one t_{short} period.

However, this ZOH discretization assumption does not hold for $k = N_s + 1, \ldots, N_p$. For these indices, a ZOH discretization would assume that the input F_{yf} is constant over one t_{long} period, shown in Fig. 3 in red. This is a poor assumption because F_{yf} can have significant variation over one t_{long} period. A better approach for the long time steps is to discrete with a FOH which assumes that the input, F_{yf}, vary linearly between time steps, as indicated in blue in Fig. 3 in blue. This provides a better approximation by avoiding the restrictive assumption that front lateral force will be piece-wise-constant over relatively long time periods. Hence, the long-term model $(k = N_s + 1, \ldots, N_p)$ can be discretized by considering the augmented state vector $\mathbf{z}_l = \begin{bmatrix} \boldsymbol{\xi} & F_{yf} & t_{\text{long}}^k \dot{F}_{yf} \end{bmatrix}^T$. The augmented state evolves according to the system:

$$\dot{\mathbf{z}}_l(k) = \begin{bmatrix} \mathbf{A}^k & \mathbf{B}^k & 0 \\ 0 & 0 & 1/t_{\text{long}}^k \\ 0 & 0 & 0 \end{bmatrix} \mathbf{z}_l(k) = \mathbf{G}_l^k \mathbf{z}_l(k) \tag{16}$$

This system can be discretized by taking the matrix exponential of $\mathbf{G}_l^k t_{\text{long}}^k$.

$$\mathbf{z}_l(k+1) = \begin{bmatrix} \mathbf{A}_l^k & \boldsymbol{\Gamma}_1^k & \boldsymbol{\Gamma}_2^k \\ 0 & 1 & 1 \\ 0 & 0 & 1 \end{bmatrix} \begin{bmatrix} \boldsymbol{\xi}(k) \\ F_{yf}(k) \\ t_{\text{long}}^k \dot{F}_{yf}(k) \end{bmatrix} \tag{17}$$

From the second row of (17) $F_{yf}(k+1) = F_{yf}(k) + t_{\text{long}}^k \dot{F}_{yf}(k)$, which is true if $\dot{F}_{yf}(k)$ is constant over t_{long}^k, verifying the FOH assumption. After making the substitutions $t_{\text{long}}^k \dot{F}_{yf}(k) = F_{yf}(k+1) - F_{yf}(k)$, the first row of (17) gives the long-term discrete model

$$\boldsymbol{\xi}(k+1) = \mathbf{A}_l^k \xi(k) + \mathbf{B}_1^k F_{yf}(k) + \mathbf{B}_2^k F_{yf}(k+1) \tag{18}$$

with $\mathbf{B}_1^k = \boldsymbol{\Gamma}_1^k - \boldsymbol{\Gamma}_2^k$ and $\mathbf{B}_2^k = \boldsymbol{\Gamma}_2^k$.

On the other hand, for the discretization of longitudinal vehicle model (6), which is a simple double-integrator, FOH method is used over the whole prediction horizon. And the discretized longitudinal dynamics can be linearly expressed as

$$\boldsymbol{\varpi}(k+1) = \begin{bmatrix} 1 & t_* \\ 0 & 1 \end{bmatrix} \boldsymbol{\varpi}(k) + \begin{bmatrix} t_*^2/2 \\ t_* \end{bmatrix} a_x(k) \tag{19}$$

where, $t*$ denotes the time step length used to discrete (6) and the subscript * represents $short$ or $long$ according to index along the prediction horizon.

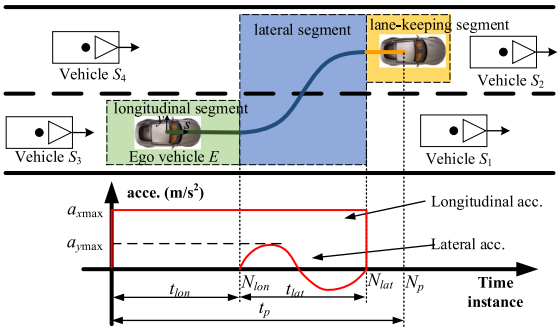

Fig. 4. Modeling of lane change process.

C. Lane Change Process Modeling

Without loss of generality, we construct a lane change scenario of an automated ego vehicle, E, traveling with four surrounding vehicles on a one-way, two-lane road. As shown in Fig. 4, vehicle S_1 and vehicle S_3 are the leading and following vehicles in the current lane, respectively. Vehicle S_2 and vehicle S_4 are the leading and following vehicles in the target lane, respectively.

To capture the lane change maneuver properties of adjusting the longitudinal position and velocity prior to initializing the lateral motion of the maneuver, a multi-segment lane change process model is proposed, as shown in Fig. 4. In the first segment, termed as the *longitudinal segment*, the ego vehicle E adjusts its longitudinal distance, position or relative velocity to find the suitable free space both in front of it and in the target lane. In the second segment, termed as *lateral segment*, E starts the lateral motion and enters into the target lane. In the third segment, termed as *lane-keeping segment*, E adjusts its relative velocity and distance to the preceding vehicle while following the target lane.

The longitudinal and lateral acceleration profiles during the lane change maneuver are deemed as constant shape and sinusoidal curve, respectively. $a_{x\max}$ and $a_{y\max}$ are the amplitude of longitudinal and lateral acceleration, respectively. $t_{\rm lon}$ and $t_{\rm lat}$ denote the duration time of the *longitudinal segment* and the *lateral segment*, respectively. A fixed prediction horizon for the lane change process is used, i.e. $t_p = 8s$. And N_p denotes the discrete time version of the prediction horizon t_p. The discrete time instants $N_{\rm lon} < N_{\rm lat} \leq N_p$ denote when E exits the *longitudinal segment* and the *lateral segment*, respectively. The *lane-keeping segment* is optional and only exists when $N_{\rm lat} < N_p$. $N_{\rm lat}$ is defined as

$$N_{\rm lat} = N_{\rm lon} + n_{\rm lat} \tag{20}$$

where $N_{\rm lon} \in \{0, 1, \ldots, N_p - n_{\rm lat}\}$, and $n_{\rm lat}$ is the discrete time version of $t_{\rm lat}$.

A finite state machine (FSM), as shown in Fig. 5, can be applied to represent the lane change maneuver flow. There are five states in this FSM, each representing a stage of the lane change maneuver. The goal state of the FSM is *lane-keeping segment* in target lane. *Lane-keeping segment* in current lane is also deemed as a goal state for traffic situations in case the lane change maneuver is suspended.

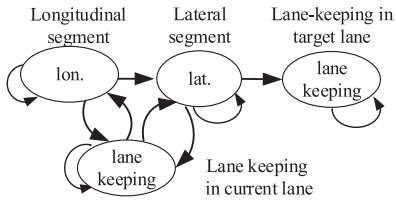

Fig. 5. The finite state machine for lane change maneuver.

III. Longitudinal and Lateral Control of Lane Change Maneuver

A. Longitudinal Control

Assuming the lateral motion of lane change maneuver is performed with a sinusoidal acceleration whose amplitude is $a_{y\max}$. Then, $t_{\rm lat}$ can be conservatively deemed as $3s$ [30]. Hence, the lane change maneuver can be perceived as primarily a longitudinal trajectory planning problem.

1) Longitudinal Safety Corridor: In terms of longitudinal trajectory planning, E must be able to traverse the previously defined three segments while maintaining safety margins to all relevant surrounding vehicles. While in the *longitudinal segment*, E must be able to maintain safety margins to the preceding vehicle S_1 and trailing vehicle S_3. Thus, $\forall k = 0 \cdots N_{\rm lon}$, the upper and lower bounds on E's longitudinal position can be defined as

$$s_{\max,k} = s_{S1,k} - s_m\left(S_{1,k}\right) \tag{21a}$$

$$s_{\min,k} = s_{S3,k} + s_m\left(S_{3,k}\right) \tag{21b}$$

Once the lateral motion of the lane change maneuver is initiated i.e., while in the *lateral segement*, E must be able to maintain safety margins to all relevant surrounding vehicles, i.e., S_1, S_2, S_3, and S_4. Thus, $\forall k = N_{\rm lon} \cdots N_{\rm lat}$, the upper and lower bounds on E's longitudinal position can thus be defined as

$$s_{\max,k} = \min\left(s_{S1,k} - s_m\left(S_{1,k}\right), s_{S2,k} - s_m\left(S_{2,k}\right)\right) \tag{22a}$$

$$s_{\min,k} = \max\left(s_{S3,k} + s_m\left(S_{3,k}\right), s_{S4,k} + s_m\left(S_{4,k}\right)\right) \tag{22b}$$

Finally, when entering the *adjusting segment*, it must be able to maintain safety margins to the preceding vehicle S_2 and trailing vehicle S_4. Hence, the upper and lower bounds on E's longitudinal position can be defined as

$$s_{\max,k} = s_{S2,k} - s_m\left(S_{2,k}\right) \tag{23a}$$

$$s_{\min,k} = s_{S4,k} + s_m\left(S_{4,k}\right) \tag{23b}$$

s_m represents the inter-vehicle safety margin, defined as

$$s_m\left(S_{j,k}\right) = v_{Sj,k}\tau + \epsilon, \forall k = 0 \cdots N_p, j = 1 \cdots 4 \tag{24}$$

where, s_{Sj} and v_{Sj} denote the longitudinal position and velocity of the jth surrounding vehicle S_j, ϵ and τ respectively denote the minimum distance and time gap which E must maintain to S_j. By allowing τ to be selected over a range from the minimum safe value to the maximum driver preferred value, it can be set to accommodate different driver styles of surrounding vehicles without compromising the safety of the automated ego vehicle,

TABLE II
DESIGN PARAMETERS FOR LONGITUDINAL MOTION PLANNING

Parameter	Range (Unit)	*Parameter*	Value (Unit)
v_x	$\{0, 30\}(m/s)$	t_{short}, t_{long}	$0.05, 0.5(s)$
a_x	$\{-3, 2\}(m/s^2)$	ϵ	$5(m)$
τ	$\{0.5, 2\}(s)$	n_{lat}	30

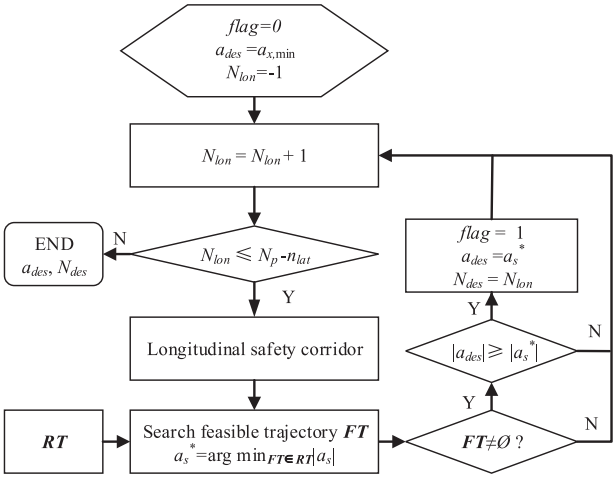

Fig. 6. Diagram for finding a feasible longitudinal solution.

E. Thus, (21)–(24) define the longitudinal safety corridor for longitudinal motion planning.

2) Longitudinal Motion Planning: The purpose of the longitudinal motion planning and control is to determine a proper time instance to initialize the lateral motion of lane change maneuver and an appropriate longitudinal trajectory for the traffic situation. The general design parameters for the longitudinal motion planning problem are given in Table II.

Utilizing the discretized longitudinal dynamics model (19) and variable time-steps t_*, the reachable set of E can crudely be approximated as a set of trajectories, *RT*. *RT* is generated by constant acceleration profiles ranging over a discrete interval from the maximum to the minimum feasible acceleration which satisfies E's physical and design limitations. The discrete interval is set to be 1% due to the finite control accuracy of the low-level controller. As such, each trajectory, $T \in RT$, can be expressed as a control sequence in terms of E's longitudinal position, s_k, velocity, $v_{x,k}$, and acceleration, $a_{x,k}$. Thus, for a longitudinal lane change trajectory to be feasible, it should satisfy the following set of constraints

$$\begin{aligned} s_{\min,k} \le s_k \le s_{\max,k} \\ v_{x\,\min,k} \le v_{x,k} \le v_{x\,\max,k} \\ a_{x\,\min,k} \le a_{x,k} \le a_{x\,\max,k} \\ \forall k = 1, \cdots, N_p \end{aligned} \tag{25}$$

Fig. 6 illustrated the algorithm to find a feasible solution.

A subset of feasible longitudinal lane change trajectories, $FT \in RT$, can thus be created by checking with (25). To allow for smooth and comfortable maneuvers, the most appropriate time instance to initialize the lateral motion of this maneuver is selected as the trajectory with corresponding time instance for which $\arg\min_{T \in FT} |a_s|$. If $FT = \emptyset$, the algorithm cannot find a feasible trajectory for E at the current situation. Then the lane change is suspended and the automated vehicle should wait for a further opportunity.

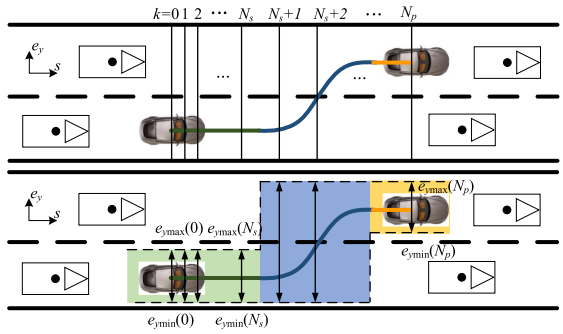

Fig. 7. Methodology to generate the lateral safety corridor.

B. Lateral Driving Safety Constraints

1) Lateral Safety Corridor: The lateral safety corridor is determined according to the longitudinal trajectory planned in the previous section and correlated to the road properties. It is represented as time-varying upper and lower bounds on E's lateral deviation (e_y) from the road centerline. The upper and lower bounds are defined by the lane boundaries, either given by the physical lane markings or virtually generated based on E's route. At each time step, the lateral trajectory of the vehicle over the prediction horizon needs to be fully contained within this corridor to ensure a safe behavior of E.

Fig. 7 illustrates the methodology to generate the lateral safety corridor. First, based on the constant longitudinal acceleration profile, the environment thus can be sampled at discrete points along the road centerline, which correspond to the vehicle's future position k steps into the prediction horizon. Then, the feasible lateral gap at each time step k is identified mainly considering the lane boundaries and vehicles effective width. Starting at the vehicle's current position and moving in the positive s direction, adjacent feasible gaps are linked throughout the prediction horizon to generate the lateral safety corridor. Therefore, the lateral safety corridor is defined as a set of lateral deviation bounds $e_{y\,\max}$ and $e_{y\,\min}$ and can be compactly written as the linear inequality:

$$H_{\text{env}} \boldsymbol{\xi}^{(k)} \le \boldsymbol{G}_{\text{env}}^{(k)} \tag{26}$$

with

$$\boldsymbol{H}_{\text{env}} = \begin{bmatrix} 0 & 0 & 0 & 1 \\ 0 & 0 & 0 & -1 \end{bmatrix}, \; \boldsymbol{G}_{\text{env}}^{(k)} = \begin{bmatrix} e_{y\,\max}^{k} - d_s \\ -e_{y\,\min}^{k} + d_s \end{bmatrix}.$$

$\boldsymbol{\xi}^{(k)}$ indicates the vehicle state at the kth time step into the prediction horizon. This provides a convex method of enforcing environmental constraints on the vehicles position. d_s is a comfort distance added to the lane marking bounds.

Note that the longitudinal safety corridor for longitudinal motion planning is determined under the assumption that E

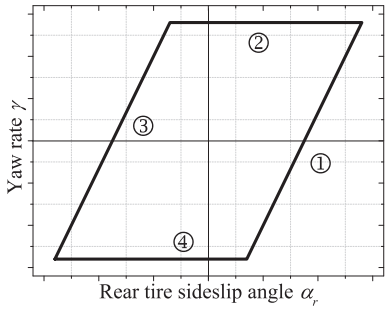

Fig. 8. Stability handling envelope for vehicle stabilization.

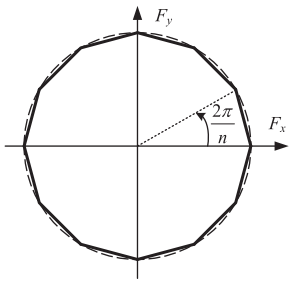

Fig. 9. Friction circle approximation with intersection of $n = 12$ half-space.

transverse the lateral segment during a conservative and fixed time duration. However, the resulted longitudinal trajectory might entail E being positioned in the lateral segment during a longer time interval. Thus, N_{lat} is redefined based on the longitudinal motion planning result, and it is expressed as

$$N_{\text{lat}*} = N_{\text{lon}} + \min\left(n_{\max}, n_{\text{lat}*}\right) \tag{27}$$

where $n_{\max}$ is the maximum allowed discrete time for laterally performing the lane change maneuver, and n_{lat*} denotes the discrete time intervals during which E is positioned in the lateral segment. In this way, the lateral safety corridor for E are set with respect to the actual time rather than the assumed time during which E is positioned in the lateral segment, thus allowing for smooth and safe maneuvers.

2) Dynamical Safety Constraints: The dynamical safety constraints are enforced as bounds on the vehicle's rear tire sideslip angle (α_r) and steady-state yaw rate (r). These bounds restrict the rear tire stays in the linear region and limit the lateral tire forces. The range of rear tire slip angle is defined from the linear tire model used in (11) and converts into a bound on vehicle states with (5b)

$$-\alpha_{r,\text{lim}} \leq \frac{v_y - l_r r}{v_x} \leq \alpha_{r,\text{lim}} \tag{28}$$

To determine an appropriate bound on yaw rate (r), a steady-state analysis is used based on (7b). This ensures that the vehicle does not exceed the linear friction region of brush tire model, and yields a maximum sustained yaw rate as:

$$r_{\text{ss,max}} = \frac{C_{\alpha r}\alpha_{r,\text{lim}}\left(1+l_r/l_f\right)}{mv_x} \tag{29}$$

The bounds (28) and (29) define a linear time-varying closed envelope, as shown in Fig. 8. (28) serves as the basis for bounds ① and ③, and ㉓ defines bounds ② and ④. Assuming real-time estimation of $C_{\alpha r}$, r, and v_x are available, the vehicle envelope described is easily calculated in real time and can be compactly represented as the following linear inequality for each time step k into the prediction horizon:

$$-\boldsymbol{G}^k_{\text{sh}} \leq \boldsymbol{H}^k_{\text{sh}}\xi^{(k)} \leq \boldsymbol{G}^k_{\text{sh}} \tag{30}$$

with

$$\boldsymbol{H}^k_{\text{sh}} = \begin{bmatrix} \frac{1}{v_x(k)} & -\frac{l_r}{v_x(k)} & 0 & 0 \\ 0 & 1 & 0 & 0 \end{bmatrix},\ \boldsymbol{G}^k_{\text{sh}} = \begin{bmatrix} \alpha_{r,\text{lim}} \\ r^k_{\text{ss,max}} \end{bmatrix}.$$

Vehicle stability is guaranteed for all states in the envelope. That is, at any point within this envelope, a steering command exists such that the vehicle can safely remain inside. Exceeding these bounds does not necessarily result in instability, but for states outside the envelope, there is no guarantee that a control input exists to move the system closer to the boundary in the next time step. Regions of the state space beyond the side slip bounds entail nonlinearity of the rear tire force, which can be difficult to control. Regions directly past the yaw rate bounds, however, do not entail tire saturation and can lead back to the handling envelope without a spin. Often vehicle states first exceed the yaw rate bound on the way to exceeding the side slip bound, which motivates using the yaw rate bound. However, small violations of the yaw rate bound by itself can occur without ensuing side slip violations, and this behavior is considered acceptable in motion control.

3) Coupled Tire Force Limitation: The limitation on coupled front tire forces can be expressed as friction circle:

$$F^2_{xf} + F^2_{yf} \leq \left(k\mu F_{zf}\right)^2 \tag{31}$$

where, $k \leq 1$ is a coefficient limiting the front tire force reach saturation. As illustrated in Fig. 9, the friction circle is modeled using the half-space approximation in a quadratic formulation. The half-space approximation is expressed as:

$$\boldsymbol{L}_y F_{yf} + \boldsymbol{L}_x F_{xf} \leq \boldsymbol{M} \tag{32}$$

$$\boldsymbol{L}_y = \begin{bmatrix} \sin\left((1)\frac{2\pi}{n} - \frac{\pi}{n}\right) \\ \sin\left((2)\frac{2\pi}{n} - \frac{\pi}{n}\right) \\ \vdots \\ \sin\left((n)\frac{2\pi}{n} - \frac{\pi}{n}\right) \end{bmatrix},\ \boldsymbol{L}_x = \begin{bmatrix} \cos\left((1)\frac{2\pi}{n} - \frac{\pi}{n}\right) \\ \cos\left((2)\frac{2\pi}{n} - \frac{\pi}{n}\right) \\ \vdots \\ \cos\left((n)\frac{2\pi}{n} - \frac{\pi}{n}\right) \end{bmatrix},$$

$$\text{and } \boldsymbol{M} = \begin{bmatrix} \cos\left(\frac{\pi}{n}\right)\mu F_{zf} \\ \cos\left(\frac{\pi}{n}\right)\mu F_{zf} \\ \vdots \\ \cos\left(\frac{\pi}{n}\right)\mu F_{zf} \end{bmatrix}$$

where, n denotes the number of half-spaces.

C. MPC Formulation for Lateral Control

The primary task of lateral control is to ensure safe vehicle operation within the previously defined constraints. This goal

is realized by express the lateral control as an optimal control problem to be evaluated over a finite prediction horizon. At each execution of the controller, the optimization problem to be solved is formulated as:

$$\underset{\boldsymbol{\xi}, F_{yf}, k=0,\cdots,N_p}{\text{minimize}} \; J = \sum_k \left(\boldsymbol{v}^{(k)}\right)^T \boldsymbol{\gamma}^{(k)} \boldsymbol{v}^{(k)} \tag{33a}$$

$$+ \sum_k \left(\boldsymbol{\xi}^{(k)}\right)^T \boldsymbol{Q}^{(k)} \boldsymbol{\xi}^{(k)} \tag{33b}$$

$$+ \sum_k \boldsymbol{\sigma}_{\text{sh}} \left| \boldsymbol{S}^{(k)}_{\text{sh,opt}} \right| \tag{33c}$$

$$+ \sum_k \boldsymbol{\sigma}_{\text{env}} \left| \boldsymbol{S}^{(k)}_{\text{env,opt}} \right| \tag{33d}$$

$$\text{s.t. } \boldsymbol{\xi}^{(\text{k}+1)} = \boldsymbol{A}^{(\text{k})}_{\text{s}} \boldsymbol{\xi}^{(\text{k})} + \boldsymbol{B}^{(\text{k})}_{\text{s}} \text{F}^{(\text{k})}_{\text{yf,opt}}$$

$$\forall k = 0, \cdots, N_s - 1 \tag{33e}$$

$$\boldsymbol{\xi}^{(k+1)} = \boldsymbol{A}^{(k)}_l \xi^{(k)} + \boldsymbol{B}^{(k)}_1 F^{(k)}_{\text{yf,opt}} + \boldsymbol{B}^{(k)}_2 F^{(k+1)}_{\text{yf,opt}}$$

$$\forall k = N_s, \cdots, N_p \tag{33f}$$

$$\left| \boldsymbol{v}^{(k)} \right| \leq \boldsymbol{v}^{(k)}_{\max} \tag{33g}$$

$$\boldsymbol{L}_y F^{(k)}_{\text{yf,opt}} \leq \boldsymbol{M} - \boldsymbol{L}_x F_{xf} \tag{33h}$$

$$\boldsymbol{H}_{\text{env}} \xi^{(k)} \leq \boldsymbol{G}^k_{env} + \boldsymbol{S}^{(k)}_{\text{env,opt}} \tag{33i}$$

$$\left| \boldsymbol{H}^k_{\text{sh}} \xi^{(k)} \right| \leq \boldsymbol{G}\boldsymbol{H}^k_{\text{sh}} + \boldsymbol{S}^{(k)}_{\text{sh,opt}} \tag{33j}$$

where $\boldsymbol{v^{(k)}} = F^{(k)}_{\text{yf,opt}} - F^{(k-1)}_{\text{yf,opt}}$.

In this formulation, the variables to be optimized are the optimal input trajectory ($F_{\text{yf,opt}}$) and the slack variables on the constraints ($\boldsymbol{S}_{\text{sh,opt}}$, $\boldsymbol{S}_{\text{env,opt}}$). And the tunable parameters are $\boldsymbol{\gamma}$, $\boldsymbol{Q}$, and the slack variable costs ($\boldsymbol{\sigma}_{\text{sh}}$, $\boldsymbol{\sigma}_{\text{env}}$). The cost function consists of four terms: (33a) establishes the trade-off between fast convergence and a smooth input trajectory, (33b) enforces penalty on the vehicle states deviation, (33c) and (33d) enforce the penalty on the slack variables violations.

The vehicle dynamics models (33e) and (33f), expressed as (15) and (19), are discretized with two-time scale prediction steps. With $\boldsymbol{v}_{\max}$ denotes the maximum allowable change in tire force, constraint (33g) reflects the physical slew rate capabilities of the vehicle steering system and (33h) reflects the maximum force capabilities of the coupled front tires. Constraints (33i) and (33j) enforce the lateral safety corridor and dynamical safety constraints, respectively. These constraints are softened with slack variables, $\boldsymbol{S}_{\text{sh,opt}}$ and $\boldsymbol{S}_{\text{env,opt}}$, to ensure a feasible solution to the optimization problem (33) always exists. With the choice of sufficiently large weighting coefficient $\boldsymbol{\sigma}_{\text{sh}}$ and $\boldsymbol{\sigma}_{\text{env}}$, cost terms (33c) and (33d) encourage zero-valued slack variables, resulting in optimal vehicle trajectories that adhere to both safe driving envelopes whenever possible.

Ideally, both constraints (33i) and (33j) can be met. However, these soften constraints ensure optimization feasibility if constraints must be violated. And along with the relative size of $\boldsymbol{\sigma}_{\text{sh}}$ and $\boldsymbol{\sigma}_{\text{env}}$, (33i) and (33j) establish a hierarchy between the collision and stabilization. Setting $\boldsymbol{\sigma}_{\text{sh}} \gg \boldsymbol{\sigma}_{\text{env}} \gg \|\boldsymbol{Q}\|_\infty$ encodes a prioritization of collision avoidance over vehicle stability and then over lane tracking. This prioritization allows the controller to selectively violate stability criteria if necessary to avoid a collision.

TABLE III
CONTROLLER AND WEIGHTS SCALING PARAMETERS

Parameter	Value (unit)	Description
Controller parameters		
N_p	25	Number of steps
N_s	10	Step for time-scale devision
$T_{s,MPC}$	0.05s	MPC execution time step
t_{short}	0.05s	Short time step size
t_{long}	0.5s	Long time step size
$\alpha_{r,lim}$	2rad	Rear tire linear region bound
Weight Normalization		
$dF_{yf,\max}$	10KN/s	Max expected input change
$e_{y\max}$	3m	Max expected lateral error
$e_{\psi\max}$	$0.15rad$	Max expected yaw angle error
$r_{\max}$	$1rad/s$	Max expected yaw rate
$v_{y\max}$	$0.17\times v_x m/s$	Max expected lateral velocity
Weight Prioritizations		
W_e	500	Environment collision slack cost
W_r	50	Yaw rate stability slack cost
W_{vy}	50	Lateral velocity stability slack cost
Q_{ey}	1	Lateral error cost
$Q_{e\psi}$	1	Heading error cost
$R_{\max}$	5	Max change in input cost

With the parameters and weights given in Table III, the optimization (33) resolves at each step using a solver generated by CVXGEN [31]. As is standard with MPC, only the optimal input for the first step into the prediction horizon, $F^{(0)}_{\text{yf,opt}}$, is used. $F^{(0)}_{\text{yf,opt}}$ converts into a steering angle using (7) before applied to the vehicle.

IV. SIMULATION RESULTS AND DISCUSSIONS

To study the performance of the proposed lane change maneuver algorithm, this section presents simulation results regarding two aspects of the algorithm. Firstly, the real-time ability of the proposed algorithm. Secondly, the capability of handling dynamical safety constraints during the lane change maneuver. Simulated lane change traffic situations are carried out in Matlab/CarSim environment.

A. Real-Time Ability

To evaluated and validated the real-time ability of the proposed lane change maneuver algorithm, it is simulated on 1000 versions of lane change traffic situations. Each test version is generated in two steps. First, a lane change traffic situation is initialized in such a way that the velocity of each vehicle is randomly selected over an interval of [5:30] m/s, and the time gap between the four surrounding vehicles to E is randomly selected over an interval of [1:8] s. Then whether there exists a minimum time window of 3 s in this randomly initialized situation is checked. Only those lane change traffic situations that satisfy the minimum time window check are adopted. As these testing scenarios are mere to illustrate the performance of the proposed lane change maneuver algorithm, the behavior of S_j

TABLE IV
MEAN AND STANDARD DEVIATION OF COMPUTATIONAL TIME IN [MS] AND THE CAPABILITY OF THE PROPOSED ALGORITHM IN [%]

	Mean	Standard	Feasible	Unfeasible
Lon. planning	12.4	0.03	93.5	6.5
Lat. control	1.8	0.002	90.5	9.5
Overall	14.2	0.31	90.5	9.5

are assumed to be constant without performing any lane change maneuvers over the prediction horizon.

The comparison results of the proposed lane change maneuver algorithm is shown in Table IV. The mean and standard deviation of the required computational time for the lane change maneuver algorithm is 14.2 ms and 0.31 ms. Then, it can be concluded that the required computational time is significantly small and remains fairly constant, which is suitable for real-time application.

From the table, it can be seen that the algorithm finds the appropriate longitudinal trajectory and corresponding time instance for initializing the lateral motion of the maneuver in approximately 93.5% of the cases. And for approximately 6.5% of the cases, it fails to find an appropriate time instance, if such exist. This failure is most likely a consequence of the constant acceleration assumption, where a large shift in the acceleration is required to find a proper solution.

Based on the results of longitudinal planning, the algorithm finds a feasible lateral trajectory in approximately 90.5% of the cases, and that approximately 9.5% of the cases are unfeasible. It only fails to find a feasible lateral trajectory, if such exist, in about 3% of the cases. The difference is most likely a result of neglecting the physical jerk constraints when planning the longitudinal trajectory for the lane change maneuver.

B. Dynamical Safety Concerns

To study the capability of handling dynamical safety constraints of the proposed algorithm, two comparison lane change scenarios are considered, referred to as Scenarios 1 and Scenario 2.

In Scenario 1, all vehicles i.e., E, S_1, S_2, S_3, and S_4, initially travels at the same longitudinal velocity, 15 m/s. From Fig. 10 it can be seen that for E to change lane in the gap between S_2 and S_4, its velocity must be reduced for it to align itself with the gap. Once E is positioned in the gap, its velocity will increase in order to maintain a safe distance to S_2 and S_4. Hence, Scenario 1 illustrates the ability of the trajectory planning algorithm for lane change maneuvers that require E to quickly decelerate into the lane change gap.

In Scenario 2, E, S_1 and S_3 initially travels at the same longitudinal velocity, 15 m/s. And S_2 and S_4 are driving at 25 m/s. From Fig. 13, it can be seen that for E to change lane in the gap between S_2 and S_4, it must increase its velocity. Hence, Scenario 2 illustrates the ability of the trajectory planning algorithm to plan lane change maneuvers which require E to accelerate into the lane change gap.

The lateral safety corridor and the corresponding lateral trajectory of the lane change maneuver for Scenarios 1 and Scenario 2 are shown in Figs. 11 and 14, respectively. In Fig. 11 it can be seen that E enters the *lateral segment* and *lane-keeping segment* at time instance 12 and 16, respectively. Fig. 14 shows that E enters the *lateral segment* and *lane-keeping segment* at time instance 2 and 5, respectively.

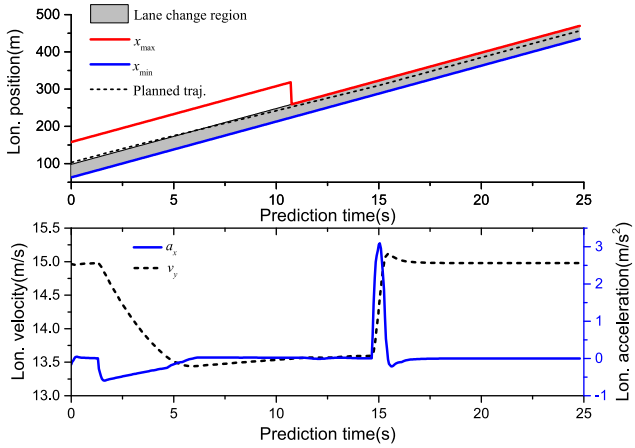

Fig. 10. Longitudinal position, velocity and acceleration of Scenario 1.

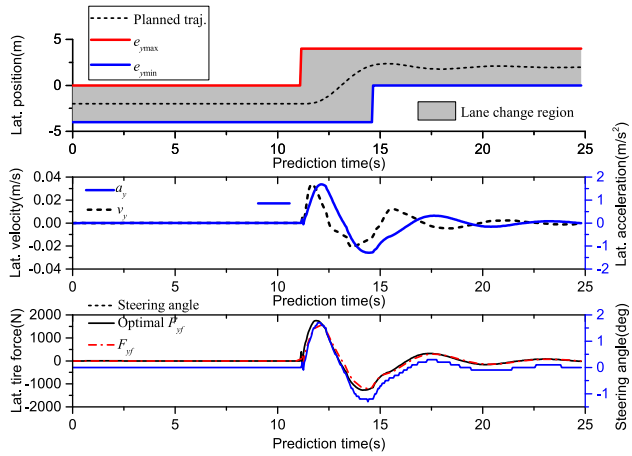

Fig. 11. Lateral position, velocity and acceleration of Scenario 1.

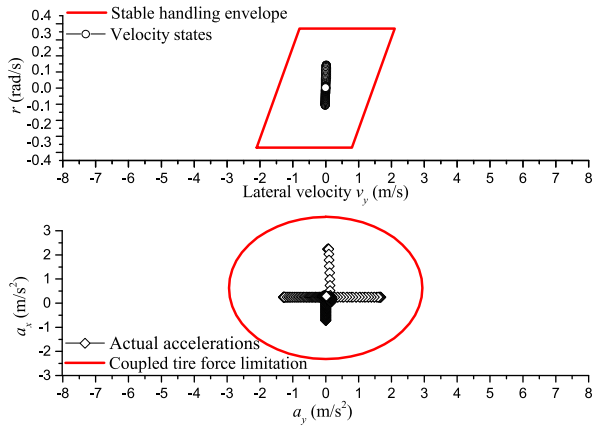

Fig. 12. Stable handling constraints and coupled tire forces of Scenario 1.

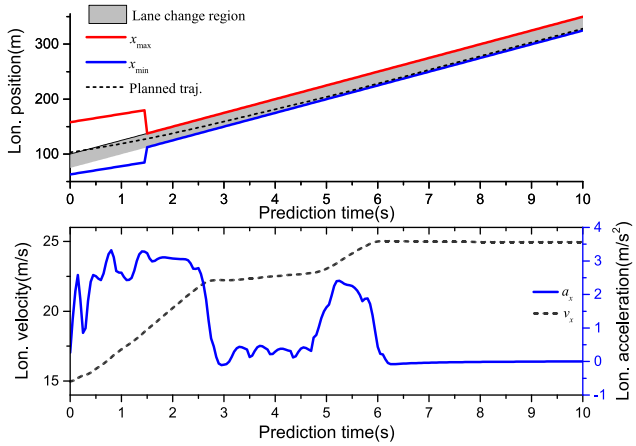

Fig. 13. Longitudinal position, velocity and acceleration of Scenario 2.

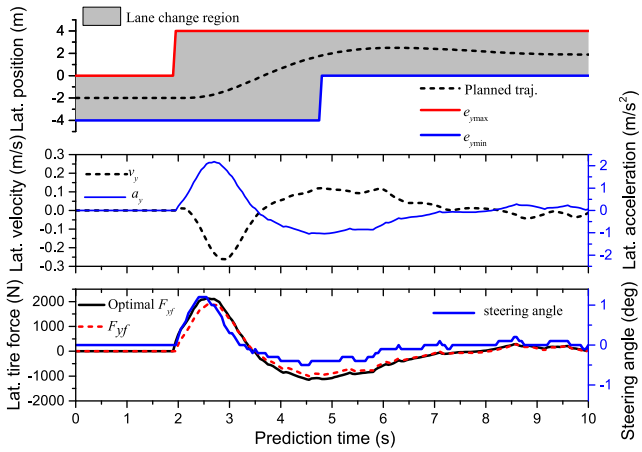

Fig. 14. Lateral position, velocity and acceleration of Scenario 2.

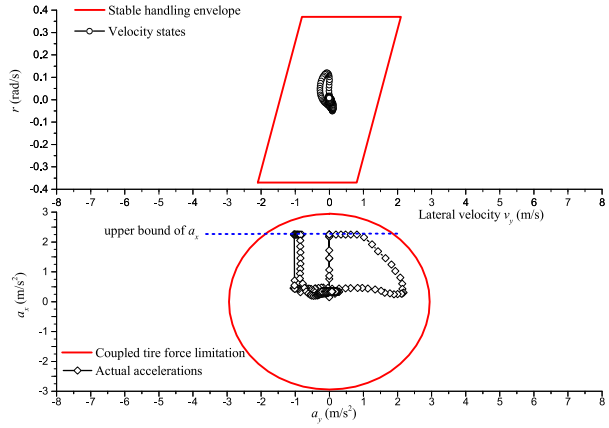

Fig. 15. Stable handling constraints and coupled tire forces of Scenario 2.

The stable handling constraints and coupled tire force limits are shown in Figs. 12 and 15. They shows the resulting lateral velocity and yaw rate which remain in the stable handling envelope. They also show the longitudinal and lateral accelerations are subjected to the coupled tire force limitations. These two examples highlight the advantage of taking dynamical safety constraints in to the optimization.

V. Conclusion

This paper presents the dynamic modeling and control of high-speed automated vehicles for lane change maneuver. Variable time-steps in prediction horizon and ZOH/FOH based discretization method are utilized to ensure a long enough prediction horizon for the lane change maneuver while maintaining model fidelity and computational feasibility. Then, considering the influence of surrounding vehicles, control of the lane change maneuver is addressed in two successive stages. First, by considering the lane change maneuver as primarily a longitudinal control problem, a velocity profile is determined. Then, the associated lateral control is generated with a model predictive controller, taking the handling stability envelope, coupled tire forces and environmental constraints into account. Simulation results demonstrate the real-time ability and stable-handling capability of the proposed approach.

To further improve the proposed lane change maneuver algorithm, future work will consider a dynamic prediction model of other traffic participations, including sensor noises and prediction uncertainties, in order to test the proposed algorithm in real-world traffic situations.

References

[1] U. Ozguner, T. Acarman, and K. Redmill, *Autonomous Ground Vehicles (ITS)*. Norwood, MA, USA: Artech House, 2011.

[2] S. Thrun *et al.*, "Stanley: The robot that won the DARPA grand challenge," *J. Field Robot.*, vol. 23, no. 9, pp. 661–692, 2006.

[3] L. Fu, A. Yazici, and U. Ozguner, "Route planning for OSU-ACT autonomous vehicle in DARPA urban challenge," in *Proc. IEEE Intell. Veh. Symp.*, 2008, pp. 781–786.

[4] J. Levinson *et al.*, "Towards fully autonomous driving: Systems and algorithms," in *Proc. IEEE Intell. Veh. Symp.*, 2011, pp. 163–168.

[5] J. H. Jeon *et al.*, "Optimal motion planning with the half-car dynamical model for autonomous high-speed driving," in *Proc. IEEE Amer. Control Conf.*, 2013, pp. 188–193.

[6] H. Zhao, C. Wang, Y. Lin, F. Guillemard, S. Geronimi, and F. Aioun, "On-road vehicle trajectory collection and scene-based lane change analysis: Part I," *IEEE Trans. Intell. Transp. Syst.*, vol. 18, no. 1, pp. 192–205, Jan. 2017.

[7] W. Yao *et al.*, "On-road vehicle trajectory collection and scene-based lane change analysis: Part II," *IEEE Trans. Intell. Transp. Syst.*, vol. 18, no. 1, pp. 206–220, Jan. 2017.

[8] Q. H. Do, H. Tehrani, S. Mita, M. Egawa, K. Muto, and K. Yoneda, "Human drivers based active-passive model for automated lane change," *IEEE Intell. Transp. Syst. Mag.*, vol. 9, no. 1, pp. 42–56, Spring 2017.

[9] B. Paden, M. p, S. Z. Yong, D. Yershov, and E. Frazzoli, "A survey of motion planning and control techniques for self-driving urban vehicles," *IEEE Trans. Intell. Veh.*, vol. 1, no. 1, pp. 33–55, Mar. 2016.

[10] C. Katrakazas, M. Quddus, W.-H. Chen, and L. Deka, "Real-time motion planning methods for autonomous on-road driving: State-of-the-art and future research directions," *Transp. Res. C, Emerg. Technol.*, vol. 60, pp. 416–442, 2015.

[11] D. Bevly *et al.*, "Lane change and merge maneuvers for connected and automated vehicles: A survey," *IEEE Trans. Intell. Veh.*, vol. 1, no. 1, pp. 105–120, Mar. 2016.

[12] J. Funke, M. Brown, S. M. Erlien, and J. C. Gerdes, "Collision avoidance and stabilization for autonomous vehicles in emergency scenarios," *IEEE Trans. Control Syst. Technol.*, vol. 25, no. 4, pp. 1204–1216, Jul. 2017.

[13] P. Hidas, "Modelling lane changing and merging in microscopic traffic simulation," *Transp. Res. C, Emerg. Technol.*, vol. 10, no. 5, pp. 351–371, 2002.

[14] M. Rahman, M. Chowdhury, Y. Xie, and Y. He, "Review of microscopic lane-changing models and future research opportunities," *IEEE Trans. Intell. Transp. Syst.*, vol. 14, no. 4, pp. 1942–1956, Dec. 2013.

[15] D. Yang, L. Zhu, B. Ran, Y. Pu, and P. Hui, "Modeling and analysis of the lane-changing execution in longitudinal direction," *IEEE Trans. Intell. Transp. Syst.*, vol. 17, no. 10, pp. 2984–2992, Oct. 2016.

[16] S. Ulbrich and M. Maurer, "Situation assessment in tactical lane change behavior planning for automated vehicles," in *Proc. Int. Conf. Intell. Transp. Syst.*, 2015, pp. 975–981.
[17] H. Tehrani, Q. H. Do, M. Egawa, K. Muto, K. Yoneda, and S. Mita, "General behavior and motion model for automated lane change," in *Proc. IEEE Intell. Veh. Symp.*, 2015, pp. 1154–1159.
[18] M. Ardelt, C. Coester, and N. Kaempchen, "Highly automated driving on freeways in real traffic using a probabilistic framework," *IEEE Trans. Intell. Transp. Syst.*, vol. 13, no. 4, pp. 1576–1585, Dec. 2012.
[19] J. Nilsson, J. Silvlin, M. Brannstrom, E. Coelingh, and J. Fredriksson, "If, when, and how to perform lane change maneuvers on highways," *IEEE Intell. Transp. Syst. Mag.*, vol. 8, no. 4, pp. 68–78, Winter 2016.
[20] J. Nilsson, M. Brnnstrm, J. Fredriksson, and E. Coelingh, "Longitudinal and lateral control for automated yielding maneuvers," *IEEE Trans. Intell. Transp. Syst.*, vol. 17, no. 5, pp. 1404–1414, May 2016.
[21] K. Hauser, "Adaptive time stepping in real-time motion planning," in *Proc. 9th Int. Workshop Algorithmic Found. Robot.*, 2010, pp. 139–155.
[22] S. J. Anderson, S. C. Peters, T. E. Pilutti, and K. Iagnemma, "An optimal-control-based framework for trajectory planning, threat assessment, and semi-autonomous control of passenger vehicles in hazard avoidance scenarios," *Int. J. Veh. Auton. Syst.*, vol. 8, pp. 190–216, 2010.
[23] G. D. Nicolao, L. Magni, and R. Scattolini, "Stabilizing receding-horizon control of nonlinear time-varying systems," *IEEE Trans. Autom. Control*, vol. 43, no. 7, pp. 1030–1036, Jul. 1998.
[24] H. Chen and F. Allgwer, "A quasi-infinite horizon nonlinear model predictive control scheme with guaranteed stability," in *Proc. Eur. Control Conf.*, Jul. 1997, pp. 1421–1426.
[25] P. Falcone, F. Borrelli, J. Asgari, H. E. Tseng, and D. Hrovat, "Predictive active steering control for autonomous vehicle systems," *IEEE Trans. Control Syst. Technol.*, vol. 15, no. 3, pp. 566–580, May 2007.
[26] E. H. Lim and J. K. Hedrick, "Lateral and longitudinal vehicle control coupling for automated vehicle operation," in *Proc. IEEE Amer. Control Conf.*, 1999, vol. 5, pp. 3676–3680.
[27] S. M. Erlien, J. Funke, and J. C. Gerdes, "Incorporating non-linear tire dynamics into a convex approach to shared steering control," in *Proc. IEEE Amer. Control Conf.*, 2014, pp. 3468–3473.
[28] C. E. Beal and J. C. Gerdes, "Model predictive control for vehicle stabilization at the limits of handling," *IEEE Trans. Control Syst. Technol.*, vol. 21, no. 4, pp. 1258–1269, Jul. 2013.
[29] J. Funke, M. Brown, S. M. Erlien, and J. C. Gerdes, "Prioritizing collision avoidance and vehicle stabilization for autonomous vehicles," in *Proc. IEEE Intell. Veh. Symp.*, 2015, pp. 1134–1139.
[30] V. A. Butakov and P. Ioannou, "Personalized driver/vehicle lane change models for ADAS," *IEEE Trans. Veh. Technol.*, vol. 64, no. 10, pp. 4422–4431, Oct. 2015.
[31] J. Mattingley and S. Boyd, "CVXGEN: A code generator for embedded convex optimization," *Optim. Eng.*, vol. 13, no. 1, pp. 1–27, 2012.

Kai Liu received the B.S. and M.S. degrees in mechanical engineering in 2008 and 2010, respectively, from the Beijing Institute of Technology, Beijing, China, where he is currently working toward the Ph.D. degree in vehicle engineering.

He is currently a Visiting Scholar with The Ohio State University, Columbus, OH, USA. His research interests include autonomous driving, vehicle dynamics modeling, intelligent vehicle systems, and model-predictive control.

Jianwei Gong received the Ph.D. degree in mechatronic engineering from the Beijing Institute of Technology, Beijing, China, in 2002.

He is currently a Professor with the Intelligent Vehicle Research Center, Beijing Institute of Technology. His research interests include planning, control, and human-like driving for autonomous vehicles.

Arda Kurt received the B.S. and M.S. degrees from Bilkent University, Ankara, Turkey, in 2003 and 2005, respectively, and the Ph.D. degree from The Ohio State University (OSU), Columbus, OH, USA, in 2011.

He is currently a Senior Research Associate with the Center for Automotive Research, OSU. His research interests include hybrid-state systems, intelligent transportation systems, autonomous vehicles, driver behavior, and driver-assistance systems.

Huiyan Chen received the Ph.D. degree from the Beijing Institute of Technology, Beijing, China, in 2004.

Since 1981, he has been with the Beijing Institute of Technology, where he is currently a Professor with the Intelligent Vehicle Research Center. His research interests include intelligent vehicle and information technologies.

Umit Ozguner received the Ph.D. degree from the University of Illinois at Urbana–Champaign, Champaign, IL, USA.

He is currently a Professor of electrical and computer engineering with The Ohio State University (OSU), Columbus, OH, USA, and holds the TRC Inc. Chair on Intelligent Transportation Systems. Since October 2013, he has been the Director of the DoT supported Crash Imminent Safety University Transportation Center, OSU. He has authored or coauthored more than 400 publications. His research interests include intelligent transportation systems, decentralized control, and autonomy in large systems.